Variant of the region-scalable fitting energy for image segmentation

Article *in* Journal of the Optical Society of America A · March 2015

DOI: 10.1364/JOSAA.32.000463

Ting-Zhu Huang
University of Electronic Science and Technol…

Hui Wang
Anshun University

Variant of the region-scalable fitting energy for image segmentation

Zhi Xu,[1] Ting-Zhu Huang,[1,*] Hui Wang,[1] and Chuanlong Wang[2]

[1]*Research Center for Image and Vision Computing/School of Mathematical Sciences, University of Electronic Science and Technology of China, Chengdu, Sichuan 611731, China*

[2]*Department of Mathematics and Computer Science, Taiyuan Normal University, Taiyuan, Shanxi 030012, China*

**Corresponding author: tingzhuhuang@126.com*

Received June 10, 2014; accepted November 18, 2014;
posted January 21, 2015 (Doc. ID 213553); published February 24, 2015

This paper presents a variant of the level set function based on region-scalable fitting (RSF) model for segmenting a given image into different parts. In consideration of the image local characteristics, the RSF model can efficiently and effectively segment images with intensity inhomogeneity. Instead of utilizing n level set functions to define up to 2^n phases in the RSF model, our method presents a piecewise constant level set formulation for image segmentation and each phase is represented by a unique constant value. In addition, our model avoids different segmentation results caused by different initializations. The energy functional of our method is locally differentiable and convex because we do not use the nondifferentiable Heaviside and Delta functions. Comparative experiment results demonstrate that our method is much more computationally efficient. Moreover, our algorithm is robust against destructive noise.

OCIS codes: (110.2970) Image detection systems; (100.2000) Digital image processing.
http://dx.doi.org/10.1364/JOSAA.32.000463

1. INTRODUCTION

Image segmentation is one of the fundamental problems in the field of image analysis and computer vision. It is a process that segments an image into disjoint subsets that correspond to their unique characteristics. In the past decades, a wide variety of segmentation methods have been proposed, such as those methods based on the level set method [1] and the graph cut [2].

The active contour model [3] proposed by Kass *et al.* does well in separating objects of interest by using an energy-minimizing method. By employing this method, we can get subpixel accuracy and a closed smooth contour. Generally speaking, active contour models can be categorized into two different classes: edge-based models [3–9] and region-based models [1,10–19]. Edge-based models use image gradient information to guide the contour toward boundaries of the desired objects. However, these models are usually sensitive to noise and weak boundaries. Compared with the edge-based models, region-based models have better performance when segmenting images with noise and weak boundaries. Region-based models utilize intensity distribution information of the image to guide the motion of the active contour. Nevertheless, most region-based active contour models assume that each region to be segmented is intensity homogeneous. For example, the Chan–Vese (CV) model [10], as a simplified version of the Mumford–Shah method [12] for segmentation, has been successfully applied for images with two regions that have a distinct mean of pixel intensity. In addition, the assumption that the intensities of images are statistically homogeneous in the CV model usually does not hold for all images.

Generally speaking, intensity inhomogeneity occurs in the vast majority of real-word images. Recently, local intensity information has been considered in the active contour methods to solve problems caused by intensity inhomogeneity. For example, Li *et al.* [16] proposed a region-scalable fitting energy (RSF) to obtain more efficient and accurate segmentation results. The RSF model introduces a kernel function K when using the local intensity information and the local intensity mean. In addition, there exist some similar methods that use local information, such as the models proposed in [11,15,20–23]. All of them perform better than the CV model on extracting objects for images with intensity inhomogeneity. Nevertheless, the RSF model is extremely sensitive to the initialization of the contour, and, in particular, if the initial position of the contour is far away from the object boundaries, the RSF model may be prone to getting stuck in local minima.

The level set method is a practical tool in image segmentation. When segmenting an image using the level set method, generally the level set is originally represented by a signed distance function. In practice, we need n level set functions when segmenting an image with 2^n phases. Later a variant of the level set formulation is introduced in [24–26]. We call this method the piecewise constant level set method (PCLSM). The work in [24–26] is to form a piecewise constant function that takes values

$$\phi = i \quad \text{in} \quad \Omega_i, \qquad i = 1, 2, \ldots, n, \tag{1}$$

where ϕ is the level set, and Ω_i represents the n disjoint regions to be segmented. This method needs only one level set function to represent several interphases and it has a lower computational cost due to the use of the augmented

Lagrangian method in solving the constrained minimization problem.

In the past few years, a new approach based on graph cuts [2,27–32] has been developed. Its basic technique is to construct a specialized graph related to the energy function so that finding the minimum cut on the graph is equal to searching for the minimization of the energy function. In fact, min-cut and max-flow problems are theoretically equivalent. Graph-based energy minimization methods arguably provide some of the most accurate solutions.

This paper presents a variant of region-scalable fitting energy (VRSF). VRSF model transforms the minimization problem of energy function with an equality constraint to an unconstrained problem by using the augmented Lagrangian method. We just need one level set in segmenting images with intensity inhomogeneity no matter how many phases there are in the image. Compared with the RSF model, our method has lower computational cost. In addition, the proposed model is robust with respect to noise.

2. BACKGROUND

A. CV Model

Based on the special case of the Mumford–Shah model [12],

$$E_{\mathrm{MS}}(u,C)=\int_{\Omega}(u(\mathbf{x})-I)^2\mathrm{d}\mathbf{x}+\nu\int_{\Omega\backslash C}|\nabla u(\mathbf{x})|^2\mathrm{d}\mathbf{x}+\mu\mathrm{Length}(C), \quad (2)$$

where $\mu\geq 0$, $\nu\geq 0$ are parameters, $u(x)$ represents the piecewise smooth image to approximate the given original image I on the image domain Ω, Chan and Vese introduced an active contour model for two-phase image segmentation. This model assumes that u is a piecewise constant function. They proposed the following energy function to be minimized as follows:

$$E_{\mathrm{CV}}(C,c_1,c_2)=\int_{\mathrm{in}(C)}(I(\mathbf{x})-c_1)^2\mathrm{d}\mathbf{x}+\int_{\mathrm{out}(C)}(I(\mathbf{x})-c_2)^2\mathrm{d}\mathbf{x}+\mu\mathrm{Length}(C), \quad (3)$$

where $\mathrm{in}(C)$ and $\mathrm{out}(C)$ represent the regions inside and outside the contour C, and c_1 and c_2 are the mean intensity values inside and outside C.

The CV model has prominent advantages in segmenting two-phase images due to its ability to acquire a larger convergence range and handle topological changes naturally. However, the CV model still has a few greater limitations in application. First, the segmentation result of the CV model largely depends on the initial contour. The final contours may be very different because of using different initial contours, especially for complicated images. Second, the CV model usually leads to poor segmentation results when dealing with images with intensity inhomogeneity. As a result, the application of the CV model is largely restricted.

B. RSF Model

The RSF model [16] proposed by Li *et al.* has considered the local distribution characteristics of intensity to deal with the problem caused by intensity inhomogeneity. In the RSF model, two fitting functions $f_1(x)$ and $f_2(x)$ are introduced to locally approximate the intensity inside and outside the contour C. At a given point $x\in\Omega$, the local intensity fitting energy is defined by

$$\varepsilon_{\mathbf{x}}(C,f_1,f_2)=\lambda_1\int_{\mathrm{in}(C)}K_\sigma(\mathbf{x}-\mathbf{y})|I(\mathbf{y})-f_1(\mathbf{x})|^2\mathrm{d}\mathbf{y}+\lambda_2\int_{\mathrm{out}(C)}K_\sigma(\mathbf{x}-\mathbf{y})|I(\mathbf{y})-f_2(\mathbf{x})|^2\mathrm{d}\mathbf{y}, \quad (4)$$

where λ_1 and λ_2 are positive constants, and $K_\sigma(u)$ is a Gaussian kernel function. To obtain the optimum boundary of the image, the total energy function

$$E^{\mathrm{RSF}}(C,f_1,f_2)=\int_{\Omega}\varepsilon_{\mathbf{x}}(C,f_1(\mathbf{x}),f_2(\mathbf{x}))\mathrm{d}\mathbf{x}+\nu\mathrm{Length}(C) \quad (5)$$

should be minimized. Insert Eq. (4) into Eq. (5) and replace C with level set ϕ, then Eq. (5) can be defined by

$$\begin{aligned}E^{\mathrm{RSF}}(\phi,f_1(\mathbf{x}),f_2(\mathbf{x}))&=\lambda_1\int\left[\int K_\sigma(\mathbf{x}-\mathbf{y})|I(\mathbf{y})-f_1(\mathbf{x})|^2H(\phi(\mathbf{y}))\mathrm{d}\mathbf{y}\right]\mathrm{d}\mathbf{x}\\&+\lambda_2\int\left[\int K_\sigma(\mathbf{x}-\mathbf{y})|I(\mathbf{y})-f_2(\mathbf{x})|^2(1-H(\phi(\mathbf{y})))\mathrm{d}\mathbf{y}\right]\mathrm{d}\mathbf{x}\\&+\nu\int|\nabla H(\phi(\mathbf{x}))|\mathrm{d}\mathbf{x}+\mu\int_{\Omega}\frac{1}{2}(|\nabla\phi(\mathbf{x})|-1)^2\mathrm{d}\mathbf{x},\end{aligned} \quad (6)$$

where the last part is a penalty term to promote the level set to approximate signed distance function and $H(x)$ is the Heaviside function.

We have an example of a two-phase image in searching for the optimum boundary. For a fixed level set ϕ, we minimize the energy functional in Eq. (6) with respect to $f_1(x)$ and $f_2(x)$, and easily obtain

$$f_i(\mathbf{x})=\frac{K_\sigma(\mathbf{x})*(M_i(\phi(\mathbf{x}))I(\mathbf{x}))}{K_\sigma*M_i(\phi(\mathbf{x}))}, \qquad i=1,2, \quad (7)$$

where $M_1(\phi)=H(\phi)$ and $M_2(\phi)=1-H(\phi)$. Keeping $f_1(x)$ and $f_2(x)$ fixed, and minimizing Eq. (6) with respect to ϕ by using the standard gradient descent method, we have the gradient flow function

$$\frac{\partial\phi}{\partial t}=-\delta(\phi)\left(\lambda_1e_1-\lambda_2e_2-\nu\,\mathrm{div}\left(\frac{\nabla\phi}{|\nabla\phi|}\right)\right)+\mu\left(\nabla^2\phi-\mathrm{div}\left(\frac{\nabla\phi}{|\nabla\phi|}\right)\right), \quad (8)$$

where $\delta(\phi)$ is the Dirac function, and e_1 and e_2 are functions defined as

$$e_i=\int_{\Omega}K_\sigma(\mathbf{y}-\mathbf{x})|I(\mathbf{x})-f_i(\mathbf{y})|^2\mathrm{d}\mathbf{y}, \qquad i=1,2. \quad (9)$$

Due to the introduction of the kernel function and the utilization of the local region information, the RSF model can accurately segment the images with intensity inhomogeneity. However, the RSF model is largely dependent on the initialization of the contour. The segmentation may need more iterations and can become time consuming if a better initial contour is not given. In addition, if the initial position of the contour is set far away from the actual boundary, the RSF model is prone to getting stuck in local minimum as a result of the nonconvexity of its energy function.

C. PCLSM

To overcome some problems caused by the traditional level set method, PCLSM was proposed in [24–26]. The PCLSM has some advantages, such as efficient computation and that it represents any number of phases with only a piecewise constant level set function:

$$\phi = i \quad \text{in} \quad \Omega_i, i = 1, 2, \cdots, n. \tag{10}$$

Based on the above assumption, the MS model can be written as

$$F(c, \phi) = \frac{1}{2}\int_{\Omega} |u - u_0|^2 \mathrm{d}\mathbf{x} + \nu \sum_{i=1}^{n} \int_{\Omega} |\nabla \psi_i| \mathrm{d}\mathbf{x}, \tag{11}$$

where $u = \sum_{i=1}^{n} c_i \psi_i$, and ψ_i, the characteristic function of the subset Ω_i, is defined as

$$\psi_i = \frac{1}{\alpha_i} \prod_{j=1, j\neq i}^{n} (\phi - j) \quad \text{and} \quad \alpha_i = \prod_{k=1, k\neq i}^{n} (i - k), \tag{12}$$

$\psi_i(x) = 1$ for any x in Ω_i, and $\psi_i(x) = 0$ elsewhere. An equation constraint,

$$K(\phi) = \prod_{i=1}^{n} (\phi - i) = 0, \tag{13}$$

is imposed to ensure that the level set ϕ takes only integer values and the image can be segmented into several disjoint regions.

By solving the minimization problem of Eq. (11) under the constraint of Eq. (13) using the augmented Lagrangian method, the energy function for this minimization problem can be written as

$$E(c, \phi, \lambda) = F(c, \phi) + \int_{\Omega} \lambda K(\phi) \mathrm{d}\mathbf{x} + \frac{\gamma}{2}\int_{\Omega} |K(\phi)|^2 \mathrm{d}\mathbf{x}, \tag{14}$$

where λ is the Lagrangian multiplier and γ is a penalty parameter. Then the saddle point for $E(c, \phi, \lambda)$ is found by means of a Uzawa-type algorithm. Next, a direct implementation of the PCLSM is presented in Algorithm 1.

Algorithm 1 Implementation of the PCLSM

Choose initial values for ϕ^0 and λ^0. For $k = 1, 2, \ldots,$ do following iterations:

1. Get c^k from $E(c^k, \phi^{k-1}, \lambda^{k-1}) = \min_c E(c, \phi^{k-1}, \lambda^{k-1})$.
2. Update $u = \Sigma_{i=1}^{n} c_i^k \psi_i(\phi^{k-1})$.
3. Get ϕ^k from $E(c^k, \phi^k, \lambda^{k-1}) = \min_\phi E(c^k, \phi, \lambda^k)$.
4. Update $u = \Sigma_{i=1}^{n} c_i^k \psi_i(\phi^k)$.
5. Update $\lambda^k = \lambda^{k-1} + \gamma K(\phi^k)$.

Remark 1. *In Algorithm 1, if there is an available initial value for c, the algorithm can first get the level set function followed by the constant values and then update the multiplier.*

3. VRSF MODEL AND ITS ALGORITHMS

In this section, we propose a method to speed up the computation based on the RSF model. A given image can be defined by a function $u:\Omega \mapsto \Re^n$, where $\Omega \in \Re^m$ is an open and bounded image domain, and $n = 1$ presents a gray level image and $n = 3$ a color image. Consider C is the boundary of the object, which separates the given image into n disjoint subdomains Ω_i. In our work, we need to find a single piecewise constant level set ϕ defined as Eq. (1) and a u defined as $u = \sum_{i=1}^{n} c_i \psi_i$ to approximate the original image. For a given point $x \in \Omega$, the local fitting energy is

$$\varepsilon_{\mathbf{x}}(c_i, \phi) = \sum_{i=1}^{n} \lambda_i \int_{\Omega_i} K_\sigma(\mathbf{x} - \mathbf{y}) |I(\mathbf{y}) - c_i(\mathbf{x})|^2 \psi_i(\phi(\mathbf{y})) \mathrm{d}\mathbf{y}, \tag{15}$$

where ψ_i is defined as Eq. (12), and $K_\sigma(x)$ is a Gaussian kernel function,

$$K_\sigma(x) = \frac{1}{(2\pi)^{n/2}\sigma^n} e^{-|x|^2/2\sigma^2},$$

where $\sigma > 0$ is a parameter. The value of $K_\sigma(\mathbf{x} - \mathbf{y})$ decreases drastically to zero when $\mathbf{y}$ goes away from $\mathbf{x}$.

If the contour C is exactly on the real object boundary and the value c_i is very close to the mean intensity value corresponding to Ω_i, the local fitting energy $\varepsilon_{\mathbf{x}}(c_i, \phi)$ can be minimized. To obtain the entire optimal boundary, we have to search for a contour C that can minimize the integral of $\varepsilon_{\mathbf{x}}(c_i, \phi)$ over the entire center point $\mathbf{x}$ in Ω. The total energy functional can be defined as

$$\begin{aligned} E(c_i, \phi) = {} & \int \sum_{i=1}^{n} \lambda_i \int_{\Omega_i} K_\sigma(\mathbf{x} - \mathbf{y}) |I(\mathbf{y}) - c_i(\mathbf{x})|^2 \psi_i(\phi(\mathbf{y})) \mathrm{d}\mathbf{y}\mathrm{d}\mathbf{x} \\ & + \nu \sum_{i=1}^{n} \int |\nabla \psi_i| \mathrm{d}\mathbf{x}, \end{aligned} \tag{16}$$

where the second part is a penalty term to smooth the contour.

To obtain a unique representation of u, and ensure that the different value in ϕ can correspond to different part of Ω, a equality constraint,

$$F(\phi) = (\phi - 1)(\phi - 2)\ldots(\phi - n) = \prod_{i=1}^{n} (\phi - i) = 0, \tag{17}$$

is introduced. The use of constraint (17) can guarantee each point $x \in \Omega$ belongs to one and only one phase Ω_i. As an example, in Fig. 1, we show the relationship between an image and the piecewise constant level set function ϕ.

Based on the above theory, the segmentation problem can be written as a constrained minimization problem:

$$\min_{\substack{c_i, \phi \\ F(\phi)=0}} E(c_i, \phi). \tag{18}$$

We use the augmented Lagrangian method to solve the problem in Eq. (18). The corresponding augmented Lagrangian functional is

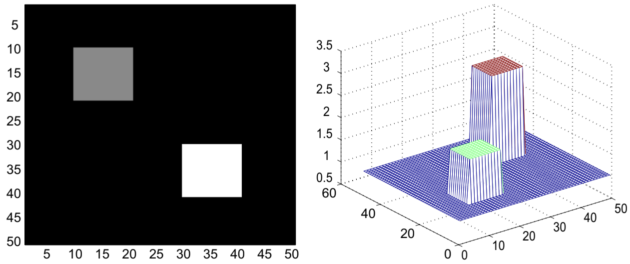

(a) (b)

Fig. 1. Relationship between an image with three phases and the piecewise constant level set function ϕ. (a) Original image and (b) the corresponding level set.

$$L(c_i, \phi, \lambda) = E(c_i, \phi) + \int \lambda F(\phi)\mathrm{d}\mathbf{x} + \frac{\gamma}{2}\int |F(\phi)|^2 \mathrm{d}\mathbf{x}, \qquad (19)$$

where γ is a positive penalty parameter, and λ is the Lagrangian multiplier. We choose a method of alternating iterative ϕ and c_i to solve Eq. (19).

We use the gradient descent method for a fixed step size Δt and c_i to obtain ϕ^k. The level set ϕ is updated as the following:

$$\phi^k = \phi^{k-1} - \Delta t \frac{\partial L(c_i, \phi^{k-1}, \lambda)}{\partial \phi}. \qquad (20)$$

The step size Δt is fixed during the whole iterative procedure. The terminal condition, which is similar to that in [24], is that

$$\left\| \frac{\partial L(c_i, \phi^k, \lambda)}{\partial \phi} \right\|_{L^2} \leq \frac{1}{10} \left\| \frac{\partial L(c_i, \phi^{k-1}, \lambda)}{\partial \phi} \right\|_{L^2}, \qquad (21)$$

or the number of iterations that is set in advance is reached.

The partial derivative of the function L is

$$\frac{\partial Ł}{\partial \phi} = \sum_{i=1}^{n} \lambda_i \int_{\Omega_i} K_\sigma(\mathbf{x}-\mathbf{y})|I(\mathbf{y}) - c_i(\mathbf{x})|^2 \frac{\partial \psi_i}{\partial \phi}\mathrm{d}\mathbf{y} - v\sum_{i=1}^{n} \nabla \cdot \left(\frac{\nabla \psi_i}{|\nabla \psi_i|}\right)\frac{\partial \psi_i}{\partial \phi} + \lambda \frac{\partial F}{\partial \phi} + \gamma F \frac{\partial F}{\partial \phi}, \qquad (22)$$

where $\frac{\partial \psi_i}{\partial \phi}$ and $\frac{\partial F}{\partial \phi}$ can be obtained from Eqs. (12) to (17).

Keeping the level set ϕ fixed, we minimize the function in Eq. (19) with respect to c_i. By calculus of variations, c_i satisfies the Euler–Lagrange equations:

$$\frac{\partial L}{\partial c_i} = \int K_\sigma(\mathbf{x}-\mathbf{y})(I - c_i)\psi_i \mathrm{d}\mathbf{y} = 0, \quad \text{for } i = 1, 2, \ldots, n. \quad (23)$$

Then from Eq. (23), c_i can be defined as

$$c_i = \frac{\int K_\sigma(\mathbf{x}-\mathbf{y}) I \psi_i \mathrm{d}\mathbf{y}}{\int K_\sigma(\mathbf{x}-\mathbf{y})\psi_i \mathrm{d}\mathbf{y}}. \qquad (24)$$

λ is updated as $\lambda^k = \lambda^{k-1} + \gamma F(\phi^k)$.

In our algorithm, we usually offer an available initial value for c_i. In this situation, we first update ϕ, followed by the constant value c_i, and then the Lagrange multiplier λ.

The detailed implementation of our VRSF model is described as follows:

- Initialize ϕ with ϕ_0 and c_i, where ϕ_0 is usually a random matrix with the same size as u_0.
- Compute ϕ^k by Eq. (20) and update $u = \Sigma_{i=1}^{n} c_i^{k-1}\psi_i(\phi^k)$.
- Compute c_i by Eq. (24) and update $u = \Sigma_{i=1}^{n} c_i^{k}\psi_i(\phi^k)$.
- Update $\lambda^k = \lambda^{k-1} + \gamma F(\phi^k)$ and check whether the termination criterion is satisfied or not. If not, $k = k + 1$ and repeat.

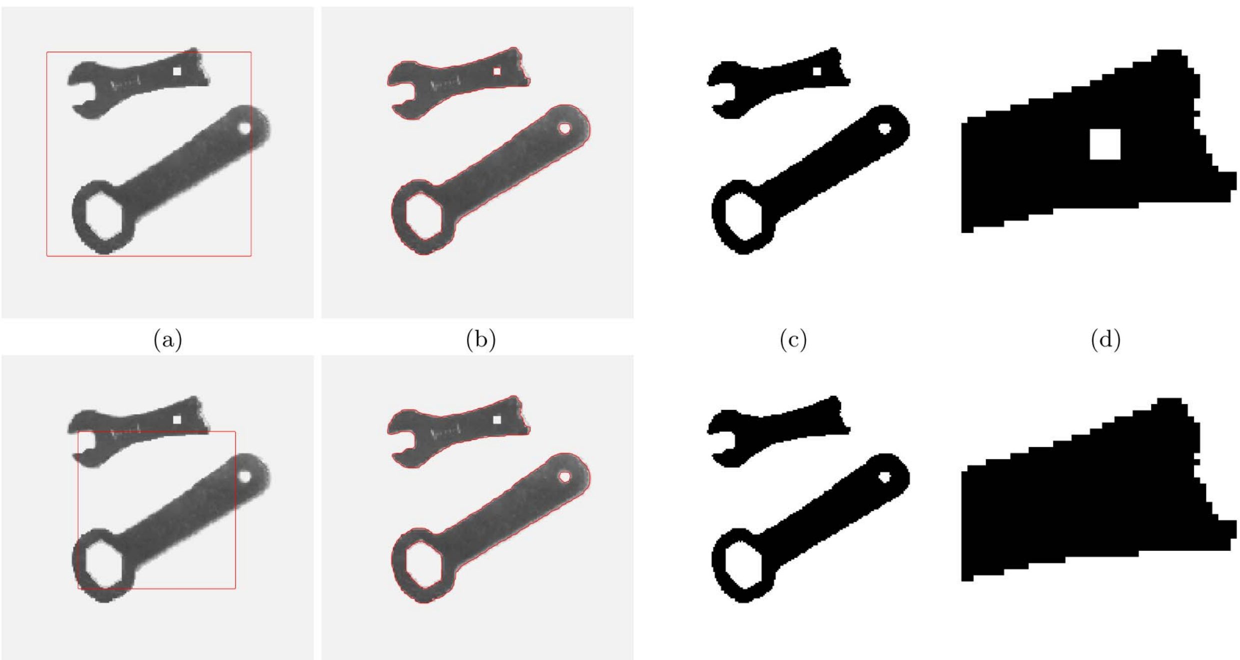

(a) (b) (c) (d)

(e) (f) (g) (h)

Fig. 2. Comparisons of the RSF model on segmentation results with different initial contours: (a) and (e) initial contours, (b) the final contour after 80 iterations, (f) the final contour after 180 iterations, (c) and (g) different phases, and (d) and (h) the different segmentation results in detail.

4. EXPERIMENTS

In this section, we mainly compare our segmentation model (VRSF) with the RSF model [16] by using real and synthetic images. Our experimental results are similar to the PCLSM. All the experiments were conducted in the MATLAB 7.0 programming environment on a computer with an Intel Core 2 Duo 2.93 GHz CPU, 2 G RAM, and the Windows XP operating system. We use a fixed parameter $\Delta t = 1e-5$ and $\gamma = 100$ for all our experiments. We choose a random matrix with the same size as the image to be segmented as the initial level set function.

First, the RSF model is used to segment a real two-phase image with size 200×200 in Fig. 2. The intensity is obvious inhomogeneity inside the object. To show the sensitivity to the initial contour for the RSF model, we segment the same image using two different initial contours. In Fig. 2, the parameters

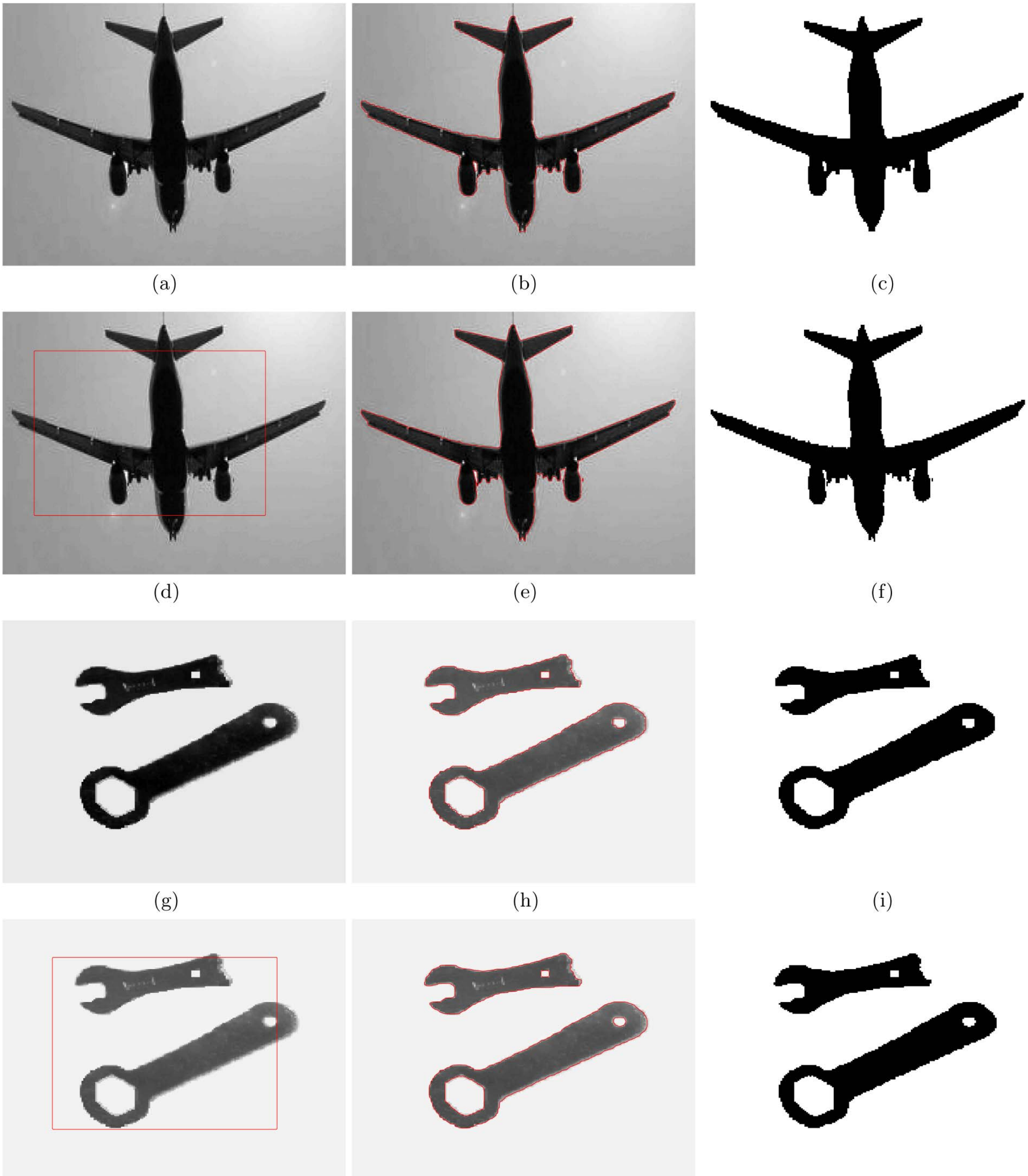

(a) (b) (c) (d) (e) (f) (g) (h) (i) (j) (k) (l)

Fig. 3. Comparisons of the RSF model and the VRSF model: Rows 1 and 3, segmentation using the VRSF model; Rows 2 and 4, segmentation using the RSF model; Column 1, original images and initial contours; Column 2, final segmentation results; Column 3, different phases corresponding to the two methods.

Table 1. Iterations and CPU Time of the Experiment in Fig. 3

	RSF [16]		Our Algorithm	
	Iterations	Time (s)	Iterations	Time (s)
Plane image	300	64.88	150	3.56
Wrench image	80	16.70	150	3.76

are set to $\mu = 1$, $\nu = 0.01 * 255^2$, and $\lambda_1 = \lambda_2 = 1$. Figures 2(a) and 2(e) are two different initial contours for the RSF model. Figure 2(b) is the final segmentation result after 80 iterations and its processing time is 15.09 s. Figure 2(f) is the final segmentation result using the initial level set Fig. 2(e) which is different with Fig. 2(a). However, it needs 180 iterations and takes 34.38 s. Figures 2(c) and 2(g) are the different phases corresponding to the two different initial level sets. Figures 2(d) and 2(h) are the different segmentation results in detail.

From the experimental results shown in Fig. 2, we can see the RSF model is extremely sensitive to the initial contour. A little change of the initial contour may cause different segmentation results and more computational cost.

Compared with the RSF model, our method can efficiently avoid the problems caused by the initialization. We need only one random matrix to define the initial level set for all images. Figure 3 illustrates the segmentation results of the RSF model and the proposed VRSF model with the same plane and wrench figures. Both models have succeeded in the segmentation. Figures 3(e) and 3(k) are the segmentation

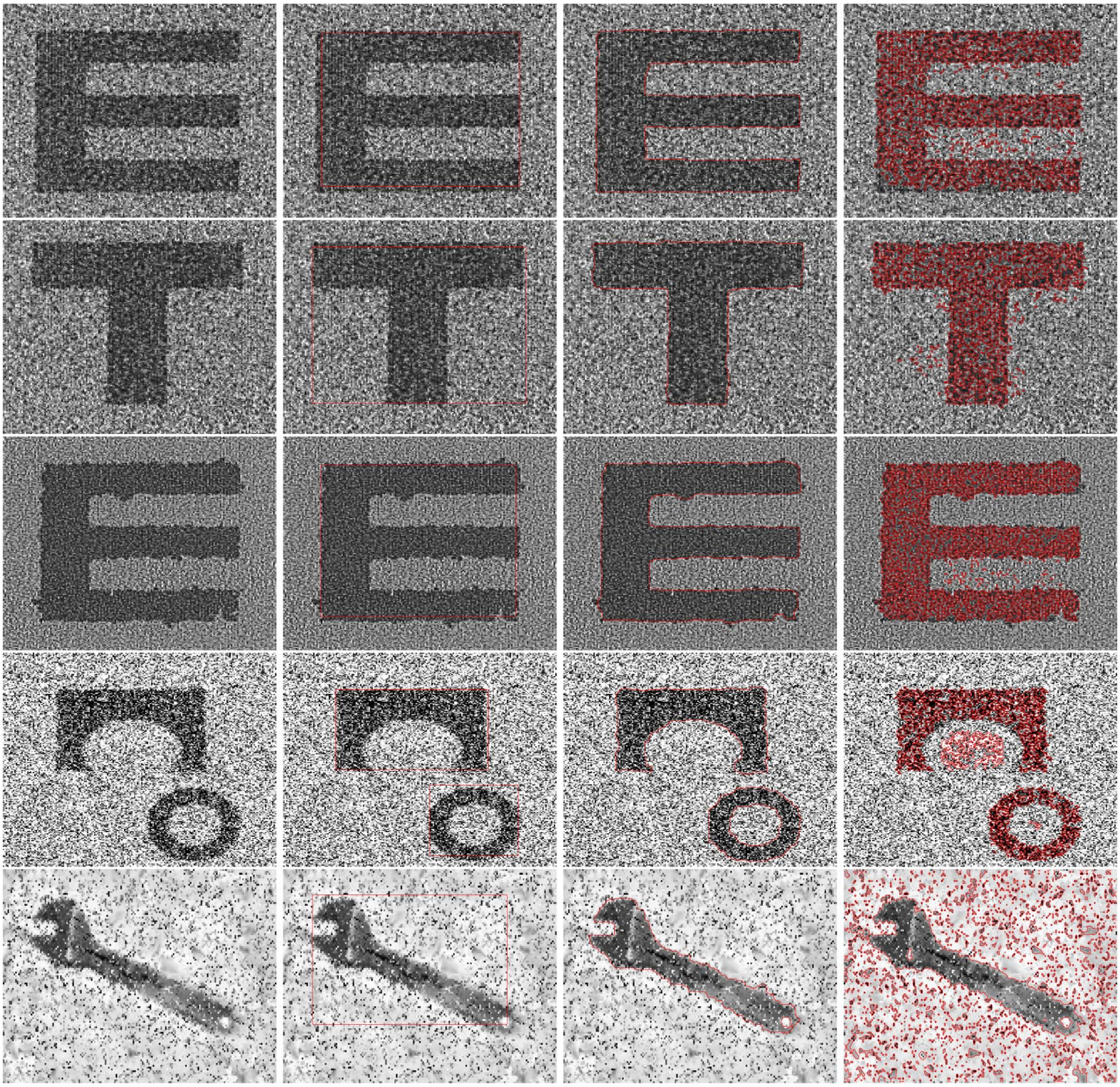

Fig. 4. Comparisons of the RSF model and the proposed VRSF model on segmenting images severely contaminated by noise: Column 1, original images; Column 2, initial contours of the RSF model; Column 3, segmentation results by the VRSF model ($\nu = 4$, $\gamma = 100$); Column 4, segmentation results by the RSF model.

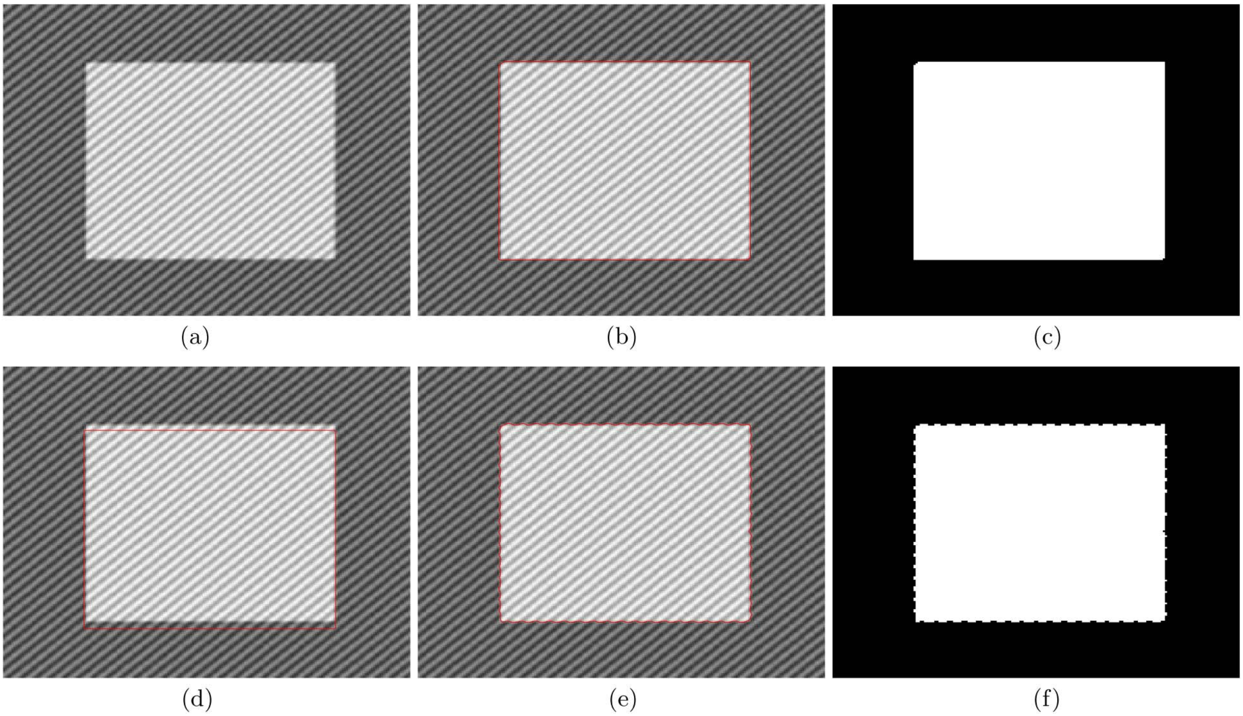

Fig. 5. Comparison of the RSF model and the VRSF model on segmenting a texture image: (a) original image, (b) and (c) segmentation result and different phases using the VRSF model, (d) initial contour of the RSF model, and (e) and (f) segmentation result and different phases using the RSF model.

results with ($\sigma = 10$, $\nu = 0.01 \times 255^2$, $\mu = 1$) and ($\sigma = 10$, $\nu = 0.001 \times 255^2$, $\mu = 1$).

However, our results do not rely on the initial position of the contour. In Figs. 3(a) and 3(g), instead of the original image with its initial contour, we show it without an initial contour. In our experiments, a smaller $\sigma = 1$ and $\gamma = 100$ is chosen, and we adjust parameter ν for different images. For example, we prefer $\nu = 2$ for Fig. 3(b) and $\nu = 4$ for Fig. 3(h). Our iteration numbers and processing time for segmentation are presented in Table 1. From Table 1, we can observe that the VRSF model consumes less time than the RSF model no matter how many iterations it needs when segmenting the same image. So the VRSF model is more efficient.

Our VRSF model can also do well in segmenting images severely contaminated by noise. Figure 4 shows the comparisons of the RSF model and our VRSF model on segmenting images severely polluted by noise. We can find that our algorithm is robust with noise. The original images are shown in column 1. It can be seen that these images are severely polluted by noise so that the edges between the different phases are obscure and the intensity in some small regions inside and outside the real contour is the same. This has increased the difficulty of segmentation. Columns 2, 3, and 4 in Fig. 4 show the initial contours of the RSF model, and the segmentation results by the VRSF model ($\nu = 4$, $\gamma = 100$) and the RSF model. It is obvious that our method has more advantages in segmenting images seriously damaged by noise. The RSF model cannot accurately distinguish the background and foreground due to the similar pixel values in the two regions, especially in row 5 of Fig. 4. Compared with the RSF model, the VRSF model is more efficient and can form closed smooth contours. Our algorithm is robust against disruptive noise.

Figure 5 shows the results of comparison of the RSF model and VRSF model on segmenting a texture image. Column 1

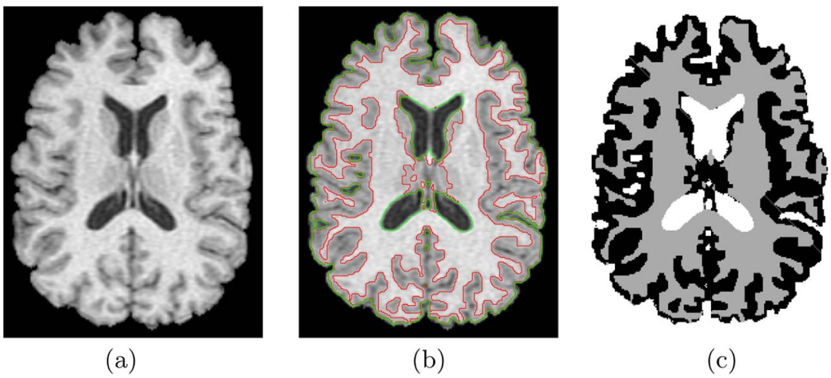

Fig. 6. Segmentation result of a three phases MR image using the VRSF model: (a) original image, (b) the segmentation result, and (c) different phases.

presents original image and the initial contour of the RSF model. Columns 2 and 3 show segmentation results and different phases corresponding to our VRSF model and the RSF model. It is not difficult to find that our method is better in segmenting texture images.

Figure 6 is the segmentation result of a three-phase magnetic resonance image (MRI) using the VRSF model. In Fig. 6, there are three tissue classes that should be identified. The three phases—cerebrospinal fluid, gray matter, and white matter—are clearly distinguished in Fig. 6(c).

5. CONCLUSION

In this paper, a VRSF and its corresponding algorithms with local Gaussian distribution fitting energies have been proposed for image segmentation. The VRSF model can efficiently segment the images with both intensity inhomogeneity and noise by employing the local region information. Meanwhile, our algorithm is time saving and robust with respect to noise. The use of the unique level set makes it convenient to segment images no matter how many phases they have. Compared with the well-known RSF model, our method is not only much more computationally efficient but also not sensitive to the initial contour.

ACKNOWLEDGMENTS

This research is supported by the 973 Program (2013CB329404), the NSFC (61370147, 61170311, 11371275), and the Fundamental Research Funds for the Central Universities.

REFERENCES

1. T. Chan and L. Vese, "Image segmentation using level sets and the piecewise constant Mumford-Shah model," Tech. Rep. CAM00-14 (UCLA Department of Mathematics, 2000).
2. E. Bae and X. Tai, "Graph cut optimization for the piecewise constant level set method applied to multiphase image segmentation," Scale Space Var. Methods Comput. Vis. **5567**, 1–13 (2009).
3. M. Kass, A. Witkin, and D. Terzopoulos, "Snakes: active contour models," Int. J. Comput. Vis. **1**, 321–331 (1988).
4. V. Caselles, R. Kimmel, and G. Sapiro, "Geodesic active contours," Int. J. Comput. Vis. **22**, 61–79 (1997).
5. R. Malladi, J. A. Sethian, and B. C. Vemuri, "Shape modeling with front propagation: a level set approach," IEEE Trans. Pattern Anal. Mach. Intell. **17**, 158–175 (1995).
6. R. Kimmel, A. Amir, and A. Bruckstein, "Finding shortest paths on surfaces using level set propagation," IEEE Trans. Pattern Anal. Mach. Intell. **17**, 635–640 (1995).
7. C. Li, C. Xu, C. Gui, and M. D. Fox, "Level set evolution without re-initialization: a new variational formulation," IEEE Comput. Soc. Conf. Comput. Vis. Pattern Recognit. **1**, 430–436 (2005).
8. C. Li, C. Xu, C. Gui, and M. D. Fox, "Distance regularized level set evolution and its application to image segmentation," IEEE Trans. Image Process. **19**, 1371–1378 (2010).
9. C. Xu and J. Prince, "Snakes, shapes, and gradient vector flow," IEEE Trans. Image Process. **7**, 359–369 (1998).
10. T. Chan and L. Vese, "Active contours without edges," IEEE Trans. Image Process. **10**, 266–277 (2001).
11. K. Zhang, H. Song, and L. Zhang, "Active contours driven by local image fitting energy," Pattern Recognit. **43**, 1199–1206 (2010).
12. D. Mumford and J. Shah, "Optimal approximation by piecewise smooth functions and associated variational problems," Commun. Pure Appl. Math. **42**, 577–685 (1989).
13. L. Vese and T. Chan, "A multiphase level set framework for image segmentation using the Mumford and Shah model," Int. J. Comput. Vis. **50**, 271–293 (2002).
14. X. Tai, A. Yezzi, and A. Willsky, "Curve evolution implementation of the Mumford-Shah functional for image segmentation, denoising, interpolation, and magnification," IEEE Trans. Image Process. **10**, 1169–1186 (2001).
15. C. Li, C. Kao, J. Gore, and Z. Ding, "Implicit active contours driven by local binary fitting energy," IEEE Comput. Soc. Conf. Comput. Vis. Pattern Recognit., 1–7 (2007).
16. C. Li, C. Kao, J. C. Gore, and Z. Ding, "Minimization of region-scalable fitting energy for image segmentation," IEEE Trans. Image Process. **17**, 1940–1949 (2008).
17. L. Wang, C. Li, Q. Sun, D. Xia, and C. Kao, "Active contours driven by local and global intensity fitting energy with application to brain MR image segmentation," Comput. Med. Imag. Graphics **33**, 520–531 (2009).
18. X. Wang, D. Huang, and H. Xu, "An efficient local Chan-Vese model for image segmentation," Pattern Recognit. **43**, 603–618 (2010).
19. J. Piovano, M. Rousson, and T. Papadopoulo, "Efficient segmentation of piecewise smooth images," Scale Space Var. Methods Comput. Vis. **4485**, 709–720 (2007).
20. C. Li, R. Huang, Z. Ding, C. Gatenby, D. Metaxas, and J. C. Gore, "A variational level set approach to segmentation and bias correction of images with intensity inhomogeneity," Med. Image Comput. Comput. Assist. Interv. **5242**, 1083–1091 (2008).
21. C. Li, C. Xu, A. W. Anderson, and J. C. Gore, "MRI tissue classification and bias field estimation based on coherent local intensity clustering: a unified energy minimization framework," Inf. Process. Med. Imag. **5636**, 288–299 (2009).
22. C. Li, C. Gatenby, L. Wang, and J. C. Gore, "A robust parametric method for bias field estimation and segmentation of MR images," IEEE Comput. Soc. Conf. Comput. Vis. Pattern Recognit., 218–223 (2009).
23. C. Li, R. Huang, Z. Ding, C. Gatenby, D. Metaxas, and J. Gore, "A level set method for image segmentation in the presence of intensity inhomogeneities with application to MRI," IEEE Trans. Image Process. **20**, 1057–7149 (2011).
24. J. Lie, M. Lysaker, and X. Tai, "A variant of the level set method and applications to image segmentation," Math. Comp. **75**, 1155–1174 (2006).
25. J. Lie, M. Lysaker, and X. Tai, "A binary level set model and some applications to Mumford-Shah image segmentation," IEEE Trans. Image Process. **15**, 1171–1181 (2006).
26. X. Tai, O. Christiansen, P. Lin, and I. Skjaelaaen, "Image segmentation using some piecewise constant level set methods with MBO type of project," Int. J. Comput. Vis. **73**, 61–76 (2007).
27. Y. Boykov and M.-P. Jolly, "Interactive graph cuts for optimal boundary and region segmentation of objects in N-D images," IEEE Int. Conf. Comput. Vis. **1**, 105–112 (2001).
28. Y. Boykov and V. Kolmogorov, "An experimental comparison of min-cut/max-flow algorithms for energy minimization in vision," IEEE Trans. Pattern Anal. Mach. Intell. **26**, 1124–1137 (2004).
29. N. Y. El-Zehiry and A. Elmaghraby, "A graph cut based active contour for multiphase image segmentation," IEEE Int. Conf. Image Process., 3188–3191 (2008).
30. E. Bae, J. Yuan, and X. Tai, "Global minimization for continuous multiphase partitioning problems using a dual approach," Int. J. Comput. Vis. **92**, 112–129 (2011).
31. J. Yuan, E. Bae, and X. Tai, "A study on continuous max-flow and min-cut approaches," IEEE Comput. Soc. Conf. Comput. Vis. Pattern Recognit., 2217–2224 (2010).
32. J. Yuan, E. Bae, X. Tai, and Y. Boykov, "A continuous max-flow approach to Potts model," Comput. Vis. **6316**, 379–392 (2010).